Regenerative Therapy 21 (2022) 307–321

Contents lists available at ScienceDirect

Regenerative Therapy

journal homepage: http://www.elsevier.com/locate/reth

Original Article

A silk fibroin/chitosan/nanohydroxyapatite biomimetic bone scaffold combined with autologous concentrated growth factor promotes the proliferation and osteogenic differentiation of BMSCs and repair of critical bone defects

Yi Zhou, Xiaoyan Liu, Hongjiang She, Rui Wang, Fan Bai, Bingyan Xiang*

Department of Orthopaedics, Third Affiliated Hospital of Zunyi Medical University (The First People's Hospital of Zunyi City), Zunyi 563000, China

ARTICLE INFO

Article history:
Received 22 March 2022
Received in revised form
22 July 2022
Accepted 17 August 2022

Keywords:
Biomimetic bone scaffold
Concentrated growth factor (CGF)
Bone marrow mesenchymal stem cells (BMSCs)
Bone regeneration

ABSTRACT

Purpose: With the goal of increasing the translational efficiency of bone tissue engineering for practical clinical applications, biomimetic composite scaffolds combined with autologous endogenous growth factors for repairing bone defects have become a current research hotspot. In this study, we prepared a silk fibroin/chitosan/nanohydroxyapatite (SF/CS/nHA) composite biomimetic scaffold and then combined it with autologous concentrated growth factor (CGF) to explore the effect of this combination on the proliferation and osteogenic differentiation of bone marrow mesenchymal stem cells (BMSCs) and the efficiency of repairing critical radial defects.

Methods: Three kinds of SF/CS/nHA composite biomimetic scaffolds with mass fractions of 3%, 4%, and 5% were prepared by vacuum freeze-drying and chemical cross-linking methods, and the characteristics of the scaffolds were evaluated. In vitro, BMSCs were seeded on SF/CS/nHA scaffolds, and then CGF was added. The morphology and proliferation of BMSCs were evaluated by live-dead staining, phalloidin staining, and CCK-8 assays. ALP staining, alizarin red staining, cellular immunofluorescence, RT–PCR, and Western blotting were used to detect the osteogenic differentiation of BMSCs. In vivo, a rabbit radius critical bone defect model was constructed, and the SF/CS/nHA-BMSC scaffold cell complex combined with CGF was implanted. The effect on bone defect repair was evaluated by 3D CT scanning, HE staining, Masson staining, and immunohistochemistry.

Results: The characteristics of 4% SF/CS/nHA were the most suitable for repairing bone defects. In vitro, the SF/CS/nHA combined CGF group showed better adhesion, cell morphology, proliferation, and osteogenic differentiation of BMSCs than the other groups ($P < 0.05$ for all). In vivo imaging examination and histological analysis demonstrated that the SF/CS/nHA scaffold combined with CGF had better efficiency in bone defect repair than the other scaffolds ($P < 0.05$ for all).

Conclusions: A SF/CS/nHA composite biomimetic bone scaffold combined with autologous CGF promoted the proliferation and osteogenic differentiation of BMSCs in vitro and improved the repair efficiency of critical bone defects in vivo. This combination may have the potential for clinical translation due to its excellent biocompatibility.

1. Introduction

Bone tissue engineering is considered the ideal method for repairing bone defects, and its three core components are seed cells with proliferation and differentiation ability, scaffold materials with good biocompatibility, and biological factors with directional differentiation ability [1–3]. However, its extremely low clinical translation efficiency is one of the problems that needs to be solved

* Corresponding author. Department of Orthopaedics, Third Affiliated Hospital of Zunyi Medical University(The First People's Hospital of Zunyi City), Fenghuang Road No.98, Huichuan District, Zunyi 563000, China. Tel: +86 18685239990.

E-mail addresses: 1322995029@qq.com (Y. Zhou), 584479028@qq.com (X. Liu), 1419925703@qq.com (H. She), 944972726@qq.com (R. Wang), 375535378@qq.com (F. Bai), xby1978@126.com (B. Xiang).

Peer review under responsibility of the Japanese Society for Regenerative Medicine.

https://doi.org/10.1016/j.reth.2022.08.006

at present. The main reason is that most synthetic materials do not have excellent biocompatibility. Although metal materials such as titanium and strontium have good osteogenic induction and mechanical properties, they have obvious cytotoxicity and refractory degradation [4]. Artificial polymer synthetic materials such as polylactic acid and polycaprolactone are degradable, but they produce acidic metabolites that inhibit cell proliferation after degradation [5]. Furthermore, many exogenous growth factors, such as BMP-2 and OPG, have obvious osteogenic induction ability, but they also induce immune rejection.

Natural bone is an inorganic–organic nanocomposite, and the layer-by-layer deposition of hydroxyapatite crystals inside collagen fibers provides bone tissue with considerable mechanical strength and superior bioactivity [6]. In this context, hydroxyapatite-natural polymer composites within the framework of organic templates are considered excellent bone biomimetic scaffolds [7]. Compared with scaffolds synthesized from other artificial materials and metal materials, such biomimetic bone scaffolds have more advantages in clinical applications because of their superior biocompatibility and excellent self–degradation properties [8,9]. Hydroxyapatite is the most important inorganic component of bone tissue. Nanoscale hydroxyapatite simulates the microstructure of human bone tissue to the greatest extent, and its fracture toughness and mechanical strength are significantly enhanced. At the same time, reduction of crystal particles makes the material's surface area larger, which is more conducive to the formation of chemical bonds with other organic framework materials [10,11]. Silk fibroin is the main component of natural silk and has been clinically used in the production of surgical sutures and artificial skin due to its low immunogenicity and good biocompatibility [12,13]. Chitosan is the only alkaline polysaccharide in natural polysaccharides. Its structure is highly similar to glycosaminoglycans in the human body, and it is perfectly compatible with the alkaline internal environment of the human body [14]. Due to the presence of free amino groups in its molecular structure, it can be combined with other biological materials for chemical modification reactions, and it has good biodegradability and cell affinity [15]. In previous research [16], we constructed an organic framework with silk fibroin (SF)/chitosan (CS) and added nanohydroxyapatite (nHA) as the main inorganic component, thereby preparing an SF/CS/nHA biomimetic composite scaffold that combined organic and inorganic components. This scaffold has been proven to have good biocompatibility, and its porosity, pore size, and mechanical strength could satisfy the basic requirements of bone defect repair.

Functional modification of scaffolds via the addition of osteogenic factors is one of the main research directions in bone tissue engineering. Numerous exogenous osteoinductive factors have been developed and utilized, such as bone morphogenetic protein-2 (BMP-2) and osteogenic growth peptide (OPG). However, exogenous growth factors are expensive, complicated to prepare, and induce immune rejection. On the other hand, bone repair is a complex and sophisticated process that is regulated by multiple factors and requires multiple growth factors to function in multiple stages. Therefore, implantation of a single exogenous growth factor has a very limited repair effect [17]. Platelets play an important role in the process of bone repair, especially during the period of hematoma inflammatory organization during fracture repair, and they can undergo self-cleavage during the inflammatory response to release a variety of endogenous growth factors [18]. Autologous platelet concentrate is a biologically active preparation extracted from the patient's blood; it is rich in a variety of endogenous growth factors, does not induce immune rejection, has excellent biocompatibility, is simple to prepare, and has a low cost [19].

CGF is the latest generation of autologous platelet concentrate biologics, and it is rich in BMP-2, vascular endothelial growth factor (VEGF), transforming growth factor-β, and other endogenous growth factors. Multiple endogenous growth factors in CGF can exert synergistic and cascading effects to enhance the induced osteogenic effect [20,21]. Different from the previous two generations of autologous platelet concentrate preparations, the preparation of CGF adopts a specific variable speed centrifugation so that the effective components of CGF can be more fully extracted [22]. CGF can form a three-dimensional fibrin network with osteoconductivity, which can provide a natural scaffold environment for local vascularization and new bone tissue growth [19]. At the same time, a larger amount of autologous growth factors is stably polymerized in the fibrin matrix, which can significantly increase the local sustained release effect of endogenous growth factors [23,24]. The release of growth factors in CGF is stable and continuous, imitating the physiological release process in the human body, so CGF is considered a natural growth factor carrier with good slow-release function [25]. Furthermore, CGF has good plasticity and compatibility so that it can be prepared into CGF extracts, lyophilized materials, CGF membranes, and CGF conditioned medium. In recent years, some studies have combined tissue engineering materials with CGF, such as CGF combined with nanohydroxyapatite, Bio-Oss bone powder, and mineralized collagen, and many results have shown good compatibility between CGF and tissue engineering materials [26–28].

Based on the current situation, the purpose of our study was to prepare an SF/CS/nHA biomimetic scaffold combined with CGF and then investigate the ability of this combination to promote the proliferation and osteogenic differentiation of bone marrow mesenchymal cells (BMSCs) in vitro and the repair effect on critical bone defects in vivo. We present the following article in accordance with the ARRIVE reporting checklist.

2. Methods and materials

2.1. Preparation and characterization of SF/CS/nHA scaffolds

Preparation of SF/CS/nHA scaffolds by vacuum freeze-drying and cross-linking [16]. Preparation of SF solution: SF was placed into a ternary solution ($CaCl_2$:H_2O:C_2H_5OH = 1:8:2) and dissolved with magnetic stirring for 1 h at 80 °C and 300 rpm. Then, the solution was dialyzed, filtered, diluted, and prepared into SF solutions with mass fractions of 3%, 4%, and 5%. Preparation of CS solution: CS was placed into 2% acetic acid solution and stirred magnetically for approximately 1 h at 100 °C and 300 rpm, and after CS was completely dissolved, CS solutions with mass fractions of 3%, 4%, and 5% were prepared. Preparation of the nHA suspension: nHA was placed into ultrapure water and stirred magnetically for 24 h at room temperature, and an nHA suspension with mass fractions of 3%, 4%, and 5% was prepared. The same mass fraction of SF solution, CS solution, and nHA suspension was mixed at a volume ratio of 1:1:1 and stirred magnetically for 3 h. Then, the mixture was transferred into a mold tank and immediately frozen at −80 °C for 24 h. Then, the samples were placed into a vacuum dryer for 24 h to shape them for the first time. The dried scaffolds were immersed in cross-linking solution (75% CH_3OH:1 mol/L NaOH = 1:1) at 4 °C for 24 h. After cross-linking, the samples were freeze-dried as before for a second shaping. Then, the dried scaffolds were immersed in a cross-linking agent (50 mmol/L EDC, 20 mmol/L NHS) and cross-linked at 4 °C for 24 h. After cross-linking, the samples were freeze-dried as before for a third shaping step. Finally, three kinds of scaffolds with mass fractions of 3%, 4% and 5% were prepared, sterilized with ethylene oxide and stored at 4 °C.

The internal structure of the scaffolds was observed by scanning electron microscopy (SEM), and the average pore diameter was

measured. The porosity was measured by a modified liquid displacement method [16]. Compressive strength and compressive modulus testing were performed with an Instron 5969 material mechanics testing machine. A preload force of 0.1 N, a load speed of 0.1 N/min, and a loading rate of 2.00 mm/min were used. The surface chemical composition of the scaffolds was detected by X-ray photoelectron spectroscopy.

2.2. Preparation of autologous concentrated growth factor (CGF)

Venous blood was drawn from the marginal ear vein of New Zealand white rabbits to prepare CGF. Five milliliters of venous blood was directly put into a 10 ml sterile test tube without anticoagulant and immediately centrifuged in a dedicated centrifuge (Medifuge) for 13 min. The specific centrifugation procedure was as follows: 30 s to accelerated, 2700 rpm for 2 min, 2400 rpm for 4 min, 2700 rpm for 4 min, 3000 rpm for 3 min, and 36 s to decelerate and stop. Centrifugation was performed to separate the blood into three layers: the plasma (PPP) was on the top layer of the tube, the fibrin-rich CGF gel layer was on the middle layer, and the bottom layer was the erythrocyte-rich RBC layer. On an ultraclean bench, a syringe was used to withdraw the top PPP, and then the CGF gel layer was separated from the RBC layer using sterile scissors. The steps for preparing CGF extract (CGFe) were as follows: the CGF gel layer was cut into pieces with sterile scissors, frozen at −80 °C for 1 h, thawed at 4 °C and centrifuged at 500×*g* for 5 min. The supernatant was aspirated and filtered and was then used as CGFe. According to previous studies on the configuration concentration of CGFe [29,30], DMEM (Solebo 31,600) was added, and the concentration of CGFe was configured to be 10%. It was stored at −80 °C. In addition, the fresh CGF gel layer was compressed with a sterile compression plate for 1–2 min to make a CGF gel membrane, which was freeze-dried and stored at −80 °C for in vivo experiments.

2.3. Investigation of the adhesion, proliferation and morphology of BMSCs

Rabbit BMSCs were provided by Procell (Cat. No.CP-Rb007, Wuhan, China). The frozen BMSCs were thawed by rapid thawing method, followed by incubation at a density of 1×10^4 cells/ml at 37 °C and 5% CO_2. The culture medium was α-MEM (Solarbio, china) with 10% fetal bovine serum (FBS,Gibco, Australia) being added. Third-generation BMSCs in logarithmic phase were observed under an optical microscope. After the SF/CS/nHA scaffolds were pretreated with sterile PBS solution containing 1% double antibody for 3 days, the scaffolds were placed horizontally in a 24-well culture plate. Third-generation BMSCs were seeded on the scaffolds at a density of 2×10^5/ml, and α-MEM containing 10% FBS was added. After culturing for 2 days at 37 °C and 5% CO_2, the scaffolds were fixed, dehydrated, dried, and sprayed with gold. Then, the morphology and adhesion of BMSCs in the scaffolds were observed by SEM.

The SF/CS/nHA scaffolds were prepared to a diameter of 2 mm and a thickness of 1 mm and were placed in a 96-well plate after sterilization. The grouping was as follows. The BM group was the control group, and only BMSCs were seeded in 96-well plates (2×10^4 cells/well). In the BM-SCN group, BMSCs were seeded on SF/CS/nHA scaffolds at a density of 2×10^4. In the BM–SCN–CGF group, BMSCs were seeded on SF/CS/nHA scaffolds, and 10% CGFe was added to the medium. Three replicate wells were set in each group. Cell proliferation was detected by the CCK-8 method on the 1st, 3rd, and 7th days. The OD values were measured at 450 nm. To detect the cytotoxicity of the scaffolds, BMSCs were seeded in 12-well plates (2×10^5 cells/well), and the groups were the same as described above. After culturing the cells for 3 days, calcein and PI (Beyotime, China) were added to each sample and incubated in the dark for 30 min. Cell viability was observed by fluorescence microscopy, and the percentage of live/dead cells was calculated. To evaluate cell morphology, phalloidin fluorescent staining solution (Beyotime, China) was added to each group after fixation with 4% paraformaldehyde. The specific method was carried out according to the instructions, and the nuclei were stained with DAPI (Solarbio, China).

2.4. BMSC osteogenic differentiation assay

2.4.1. ALP and Alizarin red staining

BMSCs were seeded in 12-well plates (2×10^5 cells/well) and grouped as above, and the a-MEM medium of each group was replaced with osteogenic induction medium (α-MEM with 10% FBS,100IU/ml penicillin/streptomycin, 10 mM β-glycerophosphate, 10 nM dexamethasone, 50 ug/mL ascorbic acid). On the 7th day, after adding 4% paraformaldehyde to fix the above three groups of samples, ALP staining was performed according to the alkaline phosphatase staining kit (Beyotime, China). On the day 21st, Alizarin Red staining was performed using Alizarin Red S stain (Solarbio, China) to assess the degree of cellular mineralization. Semiquantitative analysis was performed using Image-Pro Plus 6.0.

2.4.2. Immunofluorescence

On day 7, the expression of Runx 2 in each group of BMSCs was detected by immunofluorescence. On the 14th day, the Col-1 expression of BMSCs in each group was detected. Briefly, after fixation with 4% paraformaldehyde, permeabilization with 0.1% Triton X-100, and blocking with 5% BSA, the primary antibody was incubated overnight at 4 °C in the dark , (Runx2, Proteintech, 20700-1-AP, 1:2,00 dilution and Col-1, Proteintech, 67288-1-Ig, 1:2,00 dilution). The fluorescent secondary antibody (Proteintech 1:400 dilution) was incubated for 1 h. The nuclei were stained with DAPI (Solarbio, China). Semiquantitative analysis was performed with Image-Pro Plus 6.0.

2.4.3. Gene and protein expression

On the 14th day, total RNA was extracted from cultured cells with TRIzol (invitrogen, USA). Purified RNA was reversely transcribed into cDNA using a PrimerScript RT reagent kit (TaKaRa, Japan) under the standard conditions in accordance With the manufacturer's instructions. Then a real-time PCR kit (SYBR green PCR, Applied Biosystems, USA) was used to detect the gene expression of *Runx 2, Col-1, OCN* and *VEGF* in each group. Relative gene expression was calculated using the $2^{-\Delta\Delta}$CT method relative to GAPDH. The primer sequences are given in Table 1. On the 14th day, the protein expression levels of *Col-1, RUNX-2, OCN* and *VEGF* were detected by Western blotting in the above three groups of samples. Briefly, cells were lysed in radioimmunoprecipitation assay (RIPA) lysis buffer. Equal amounts of protein samples were evaluated using a BCA protein kit (Beyotime, China). After separation via sodium dodecyl sulfate–polyacrylamide gel electrophoresis (SDS–PAGE), proteins were transferred to polyvinylidene fluoride (PVDF) membranes (Millipore, MA, USA), followed by blocking with 5%

Table 1
Primers used for RT–PCR.

Gene	Forward	Reverse
Runx 2	TGACCAGCAGGCAGGAAACA	TCTCACAGCATCCTACGCCG
Col-1	TTGGTGTGGCGTCCATGAGT	ACACGCAGCTGGTCAGACAT
OCN	AGTCTGGCAGAGGCTCAGGTAC	GGTCAGGTGGTTGTAGGCTTGG
VEGF	AGGACTATGCTGGTTCCCGC	ATCTCCAGGCTGTTCCGAGC
GAPDH	CGAGCTGAACGGGAAACTCA	CCCAGCATCGAAGGTAGAGG

RT–PCR, reverse transcription-polymerase chain reaction.

nonfat milk. All primary antibodies were incubated at 4 °C overnight. The immunocomplexes were incubated with horseradish peroxidase-linked secondary antibodies (1:5000 dilution) at room temperature for 1 h. After exposure, the strips were quantified with ImageJ 1.6.0. The primary antibodies were used as follows: *Col-1* (Proteintech, 67288-1-Ig, 1:2000 dilution), *Runx2* (Proteintech, 20700-1-AP, 1:2000 dilution), *OCN* (Abcam, ab133612, 1:1000 dilution), *VEGF* (Proteintech, 19003-1-AP, 1:2000 dilution).

2.5. Repair of critical radial defects

2.5.1. Surgical procedure

The animal experiment was approved by the Institutional Animal Care and Use Committee of our university (IRB No. 2021-2-373). Four-month-old New Zealand white rabbits (body weight 3.5–4.0 kg) were used in the in vivo experiments. The rabbits were anesthetized by intramuscular injection with xylazine hydrochloride (0.025 ml/kg). According to some studies on critical radial defects [31,32],a longitudinal incision was created in the middle of the right radius to fully expose the radius, and a 15 mm long, 3 mm diameter cylindrical bone defect was created in the middle of the radius with a microvibrating saw. The SF/CS/nHA-BMSCs scaffold cell complexes were prepared as follows:The SF/CS/nHA scaffolds were prepared to a diameter of 3 mm and a length of 15 mm.Third-generation BMSCs were seeded on the scaffolds at a density of 2×10^5/ml, and α-MEM containing 10% FBS was added. Then the SF/CS/nHA-BMSCs scaffold cell complexes were prepared after culturing for 3 days at 37 °C and 5% CO_2 for the further vivo experiments.Eighteen rabbits were divided into 3 groups by the random number table method: the BM group was the control group, and only BMSCs were implanted at the stump of the bone defect (n = 6); the BM-SCN group was implanted with SF/CS/nHA-BMSCs scaffold cell complexes at the bone defect site (n = 6); in the BM–SCN–CGF group (n = 6), the SF/CS/nHA-BMSC scaffold cell complex was implanted at the bone defect site, and then the CGF gel film was completely coated on the surface of the SF/CS/nHA scaffold, which was similar to the Masquelet membrane induction technique [33]. The nondegradable bone marrow mud in Masquelet technology was replaced with the SF-CS-nHA biomimetic biodegradable scaffold. CGF membrane acted as an inducing membrane. Furthermore, the BM–SCN–CGF group was injected with 1 ml 10% CGFe into the surgical area weekly with a 5 ml syringe. The incision was sutured layer by layer, and the rabbit received intramuscular injection with penicillin for 3 days to prevent infection.

2.5.2. Radiological assessment

A 3D CT (SOMATOM Definition AS, Siemens, Germany) scan was performed on all model animals at the surgical site in postoperative weeks 4, 8, and 12. Three-dimensional reconstruction was carried out with a 1 mm layer thickness. Bone mineral density (BMD) at the bone defect site was calculated by using QCT Pro software (Image Analysis QCT, Mindways, American). The sagittal images of the middle layer were selected to calculate the Lane-Sandhu Radiology Score.

2.5.3. Histopathological assessment

At 12 weeks postoperatively, the rabbits were sacrificed by anesthesia with an overdose of xylazine. The radius of the operated side was removed, fixed with paraformaldehyde, decalcified with EDTA, dehydrated with alcohol, embedded in paraffin and cut into 5 μm sections for hematoxylin and eosin (HE) staining and Masson staining. The expression of Col-1 (Proteintech, 67288-1-Ig, 1:200 dilution) and CD31 (Proteintech, 11265-1-AP, 1:100 dilution) in each group was detected by immunohistochemistry. Briefly, antigen retrieval, blocking, incubation with primary antibody, secondary antibody, DAB color development, and hematoxylin counterstaining were performed in sequence. In addition, tissue immunofluorescence was used to further verify the expression of Col-1 in bone tissue of each group after antigen retrieval (the method is the same as that described above). The above results were semiquantitatively analyzed by using Image-Pro Plus 6.0.

2.6. Statistical analysis

Quantitative experimental results are expressed as the mean ± standard deviation. Each experiment was replicated at least 3 times. The data were analyzed using SPSS (version 26.0; IBM Corp., Armonk, NY). One-way analysis of variance (ANOVA) was used for comparisons between multiple groups. Post hoc comparisons were made using the Bonferroni method. A P value < 0.05 was considered statistically significant.

3. Results

3.1. Characterization of SF/CS/nHA scaffolds

The 3%, 4%, and 5% SF/CS/nHA scaffolds showed no significant differences in appearance. They were solid white cylinders, which could be shaped as needed. They had obvious compression resistance and elasticity. The cutting surface of the scaffolds was smooth and flat. The microstructures of the three kinds of SF/CS/nHA scaffolds under SEM showed that nHA was uniformly deposited on the organic framework composed of SF and CS. The inner pores of the scaffold were uniform. The inside of the scaffolds were stable three-dimensional mesh structures, which could provide sufficient space for cell adhesion and growth. The average pore diameters of the 3%, 4%, and 5% scaffolds were 146.53 ± 22.43 μm, 126.53 ± 16.11 μm, and 96.53 ± 13.01 μm, respectively. The average porosities were 89.33 ± 2.01%, 83.173 ± 2.37%, and 78.46 ± 1.74%, respectively. The average porosity and pore size gradually decreased with increasing mass fraction. The average compressive modulus of the 3%, 4%, and 5% scaffolds were 0.45 ± 0.11 MPa, 0.77 ± 0.14 MPa, and 0.91 ± 0.18 MPa, respectively. The average compressive strengths of these scaffolds were 4.81 ± 0.47 MPa, 6.84 ± 0.63 MPa, and 8.13 ± 0.71 MPa, respectively. The average compressive strength and compressive modulus increased with increasing mass fraction. Ion spectroscopy analysis showed that the main components of the three scaffolds were C and O, and the scaffolds also contained abundant Ca and P necessary for bone mineralization. Although the 5% scaffold had the highest mechanical strength, the porosity was lower, while the 3% scaffold had the lowest mechanical strength. Therefore, we chose the 4% scaffold for subsequent experiments after comprehensive comparison. The characterization of the SF/CS/nHA scaffold is shown in Fig. 1.

3.2. Preparation of concentrated growth factor

As shown in Fig. 2, a specific differential centrifugation procedure is used to separate the blood into three layers: anemic plasma (PPP layer) in the top layer of the tube, a fibrin-rich gel in the middle layer (CGF layer), where platelets and concentrated growth factors are captured, and red blood cells (RBC layer) in the bottom layer (Fig. 2A). After mechanical separation, CGF gels were prepared (Fig. 2B), further freeze–thawed, centrifuged again, and diluted with sterile PBS to prepare 10% CGFe (Fig. 2C).

3.3. Examination of BMSC adhesion, proliferation and morphology

Under the microscope, the third-generation BMSCs were spindle-shaped in the culture plate, and the cell colonies were swirl-like (Fig. 2E). In the SF/CS/nHA scaffolds, a large number of

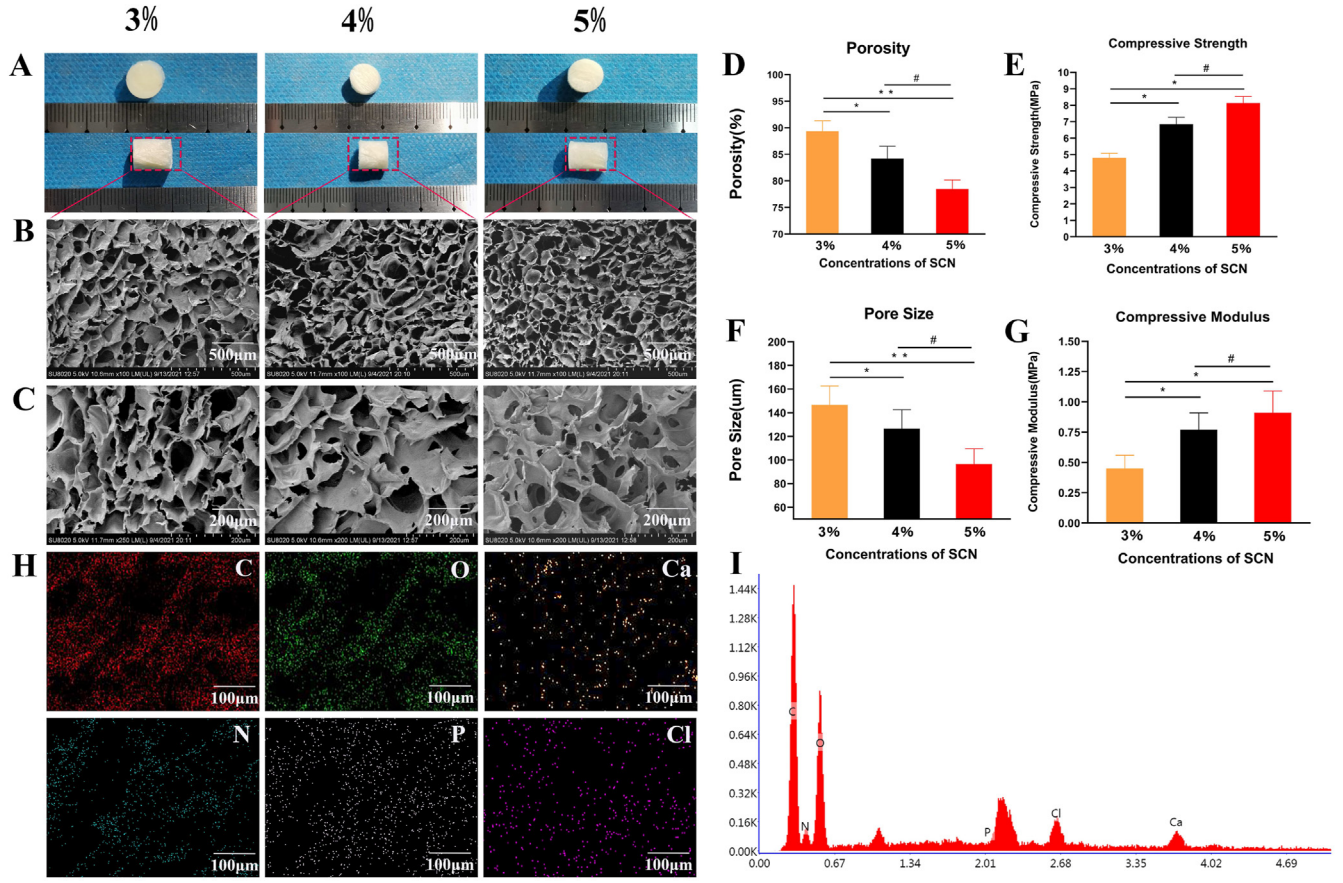

Fig. 1. Characterization of the SF/CS/nHA scaffold (A) Appearance of the SF/CS/nHA scaffold (B–C) SEM image of SF/CS/nHA scaffold (D–G) relevant parameters of the SF/CS/nHA scaffold (H–I) energy dispersive spectrometry analysis of the SF/CS/nHA scaffold. SEM, scanning electron microscopy.

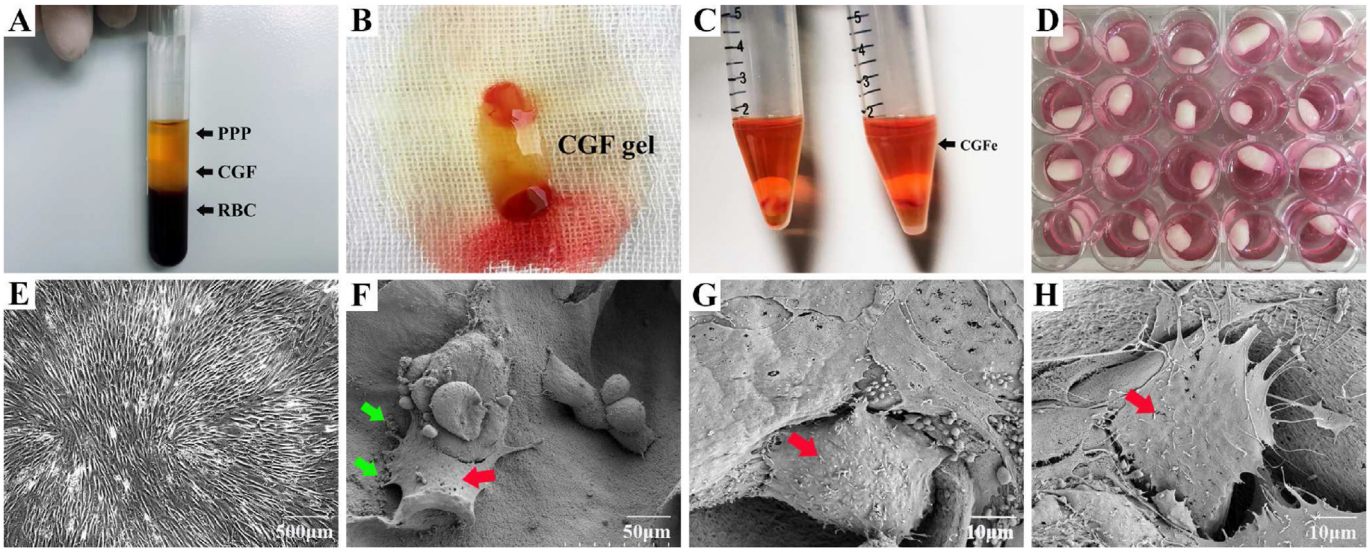

Fig. 2. Preparation of CGF, cell culture and cell adhesion in scaffolds (A–C) Preparation of CGF (D) BMSC culture in the SF/CS/nHA scaffold (E) light microscopy image of BMSCs (F–H) SEM image of BMSCs in the SF/CS/nHA scaffold; SEM, scanning electron microscopy; Red Arrow, BMSCs; Green Arrow, calcium crystals.

BMSCs were observed to adhere to the surface and pores of the scaffolds, with a flat or oval shape, growing in clusters, with cells with protruding pseudopodia, secreted vesicles, and some calcium salt crystals formed by nHA wrapping around the cells. This indicated that the cells adhered and grew well on the scaffolds (Fig. 2F–H). The results of live/dead staining showed that a large number of viable BMSCs were found in all three groups, and only a very small number of dead cells were observed (Fig. 3A). The proportion of viable cells was as follows: BM group: 92.3 ± 3.7%, BM-SCN group: 89.5 ± 2.6%, and BM–SCN–CGF group: 94.7 ± 2.1%.

There was no significant difference in the proportion of viable cells among the three groups (P = 0.31) (Fig. 3B). This result indicated that the scaffold components and 10% CGFe had no obvious cytotoxicity. The results of phalloidin staining showed that after 3 days of culture, all three groups exhibited cell adhesion and growth, but the BM-SCN group had the smallest number of cells, the smallest degree of cell extension, and the smallest coverage area among the three groups. In the BM–SCN–CGF group, the cells were more numerous, spread well, and covered a large area, the cellular actin filaments were clearly visible, and the morphology was the closest to that of the BM group seeded in the culture plate (Fig. 3C). The results of CCK-8 assays showed that on the first day, there was no significant difference in cell proliferation among the groups (P = 0.23). On the 3rd and 7th days, the BM–SCN–CGF group showed a significant trend of cell proliferation compared with the other two groups (P < 0.01) (Fig. 3D).

3.4. BMSC osteogenic differentiation assay

ALP staining reflected the early osteogenic differentiation effect on cells, and Alizarin red staining detected the mineralization degree of cells at the late stage of osteogenesis. Semiquantitative analysis with Image-Pro Plus 6.0 showed that the depth and area of the BM–SCN–CGF group were significantly higher than those of the other two groups in terms of ALP staining and alizarin red staining (P < 0.05), while the values of the BM-SCN group were significantly higher than those of the BM group (P < 0.05) (Fig. 4).

The expression of the osteogenesis-related proteins *Runx-2* and *Col-1* in BMSCs in each group was evaluated by cellular immunofluorescence. Semiquantitative analysis with Image-Pro Plus 6.0 showed that after 7 d of osteoinduction, the fluorescence intensity of *Runx-2* protein in the BM–SCN–CGF group was significantly higher than that in the other two groups (P < 0.05), and the fluorescence intensity in the BM-SCN group was significantly higher than that in the BM group (P < 0.05). The same results were obtained for the *Col-1* protein after 14 d of osteoinduction (Fig. 5).

Furthermore, we explored the osteogenic differentiation effect on BMSCs at the gene and protein levels. The expression levels of the osteogenesis-related genes *Runx-2*, *OCN* and *Col-1* were significantly increased in the cells of the BM–SCN–CGF group compared with the cells of the other two groups after 14 d of osteoinduction (P < 0.05), and the values of the BM-SCN group were significantly higher than those of the BM group (P < 0.05) (Fig. 6). Notably, the expression of the angiogenesis-related gene VEGF was upregulated only in the BM–SCN–CGF group, and there was no difference between the other two groups. This result indicated that CGF may have a unique proangiogenic effect. Furthermore, we used Western blotting to detect the protein expression of the above genes and used ImageJ to quantitatively analyze the expression data. The results were consistent with the RT–PCR results.

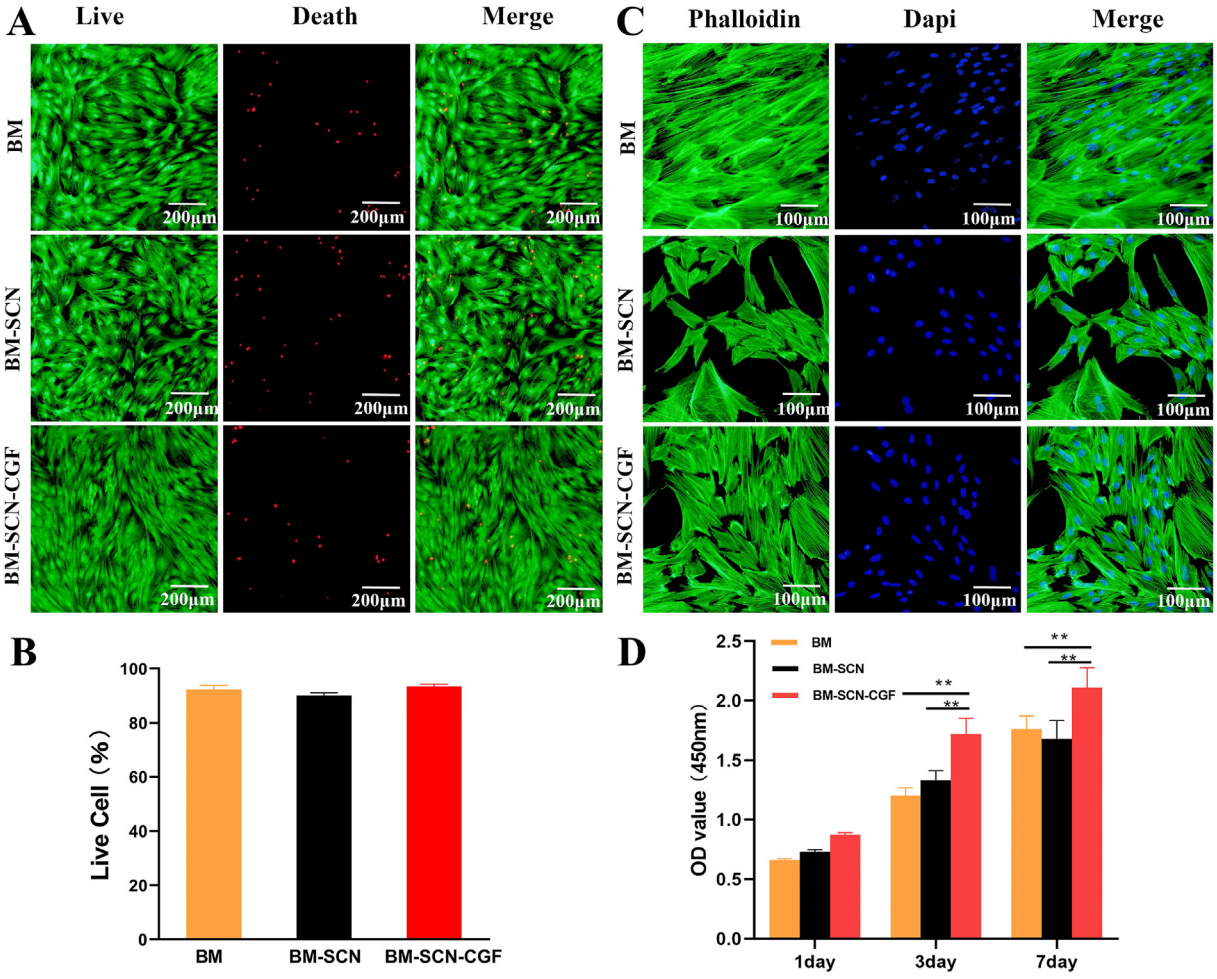

Fig. 3. BMSCs proliferation and morphology detection (A) Live/dead staining of BMSCs (B) the percentage of living BMSCs among the three groups (n = 3) (C) microfilament skeleton of BMSCs stained with phalloidin (D) the CCK-8 assays showing the proliferation ability of BMSCs among the three groups (n = 4). *p < 0.05, **p < 0.01, ***p < 0.001 compared with the BM–SCN–CGF group.

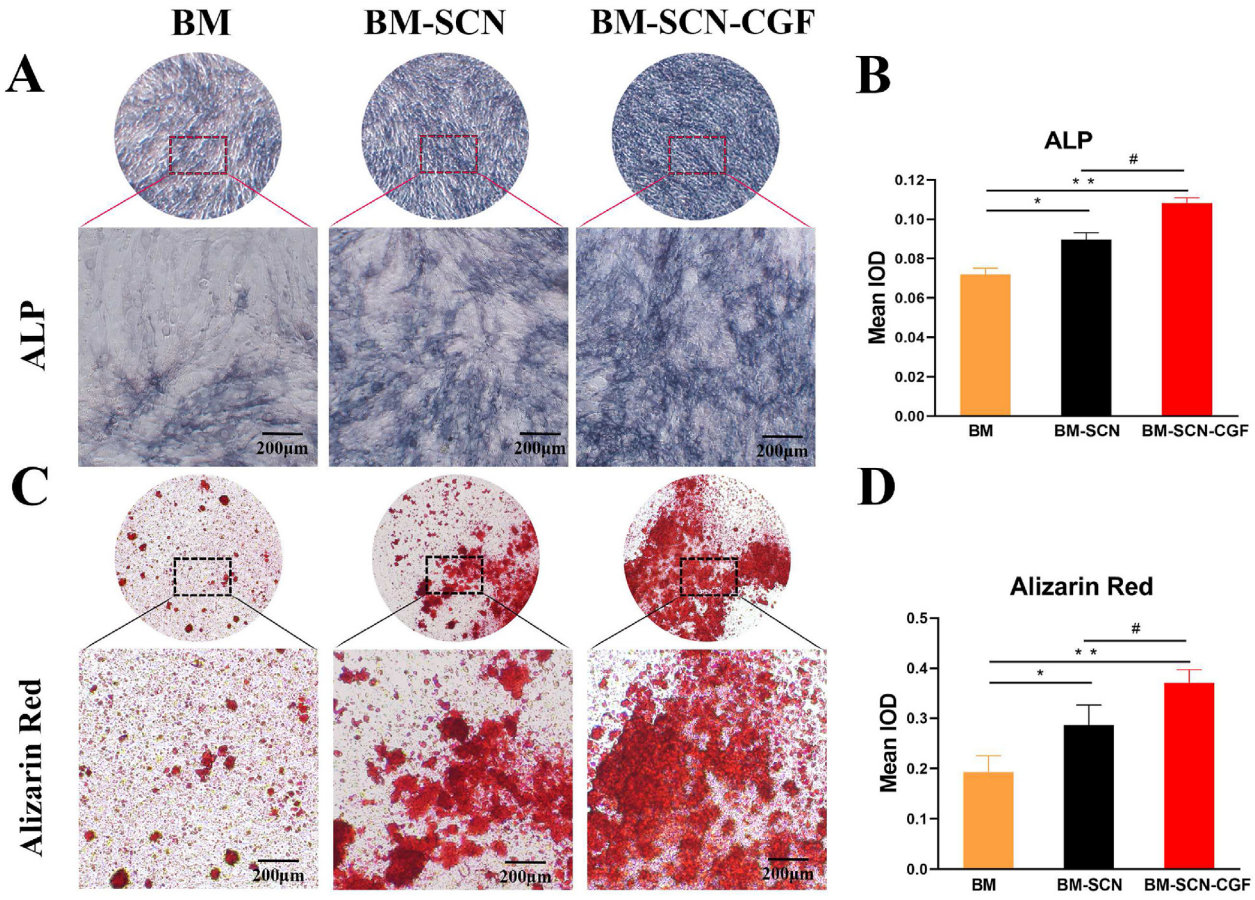

Fig. 4. ALP staining and Alizarin red staining (A) ALP staining images of BMSCs under a microscope after 7 d of osteoinduction (B) Quantitative results of ALP staining (n = 4) (C) Alizarin red staining images of BMSCs under a microscope after 21 d of osteoinduction (D) Quantitative results of Alizarin red staining (n = 4). ALP, alkaline phosphatase; IOD, integrated optical density; *p < 0.05, **p < 0.01 compared with the BM group, #p < 0.05 compared with the BM-SCN group.

3.5. Repair of critical radial defects

All animals recovered well from the surgical procedure. No infections or other complications were observed. The surgical process is shown in Fig. 7A–F. The gross observation results showed that there was still an obvious bone defect in the BM group, a partial bone defect in the BM-SCN group, and almost complete repair of the bone defect in the BM–SCN–CGF group (Fig. 7G–I).

The repair of bone defects was evaluated by 3D CT at 4, 8, and 12 weeks after the operation (Fig. 8A). At 4 weeks, no obvious repair was found in the BM group, a small amount of new bone formation was seen at the broken end of the bone defect in the BM-SCN group, and part of the bone defect area was repaired in the BM–SCN–CGF group. At 8 weeks, there was a slight increase in new bone at the edge of the bone defect area in the BM group, and part of the new bone grew from the broken end to the center in the bone defect area in the BM-SCN group, but an obvious bone defect area was still observed. However, in the BM–SCN–CGF group, a large amount of new bone filled the bone defect area, and fracture ends almost healed, leaving only a small bone defect area. At 12 weeks: In the BM group, an obvious bone defect area was still seen, and the medullary cavity was occluded. In the BM-SCN group, the bone defect area was basically healed, but compared with those of normal bone tissue, the bone density was lower, and the continuity of the bone cortex was poor. In the BM–SCN–CGF group, there was no significant difference between the repaired bone defect area and normal bone tissue, while the bone marrow cavity was basically completely recanalized, and the bone cortex was continuous. Furthermore, the L-S score and BMD values of the BM–SCN–CGF group were higher than those of the other two groups at 4, 8, and 12 weeks ($P < 0.01$) (Fig. 8B and C).

As shown in Fig. 9, HE staining and Masson staining at 12 weeks showed that in the BM–SCN–CGF group, most of the implanted SF/CS/nHA scaffolds were degraded, a large amount of new bone was formed, the bone trabeculae were neatly arranged, some bone trabeculae had formed woven bone, and there was an obvious transition zone between the remaining scaffold and the new bone. The new bone was integrated well with the scaffold. BM-SCN group: The implanted SF/CS/nHA scaffolds were partially degraded, and some new bone was formed, but the arrangement of bone trabeculae was disordered. Some of the remaining scaffolds were surrounded by fibrous tissue, with a clear boundary with the new bone. There was poor integration of the scaffold with new bone tissue. In the BM group, almost no new bone tissue was formed, and a large amount of fibrous tissue was formed in the bone defect area. Type I collagen (Col-I) is an important component in the development of bone mechanical strength, and CD31 is a specific protein involved in angiogenesis. In the 12th week, we detected the expression of COL-1 and CD31 by immunohistochemical staining and used Image-Pro Plus 6.0 for semiquantitative analysis. The results showed that the expression of Col-I and CD31 in the BM–SCN–CGF group was significantly higher than the other two groups ($P < 0.01$). The values in the BM-SCN group was significantly higher than those in the BM group ($P < 0.05$). In

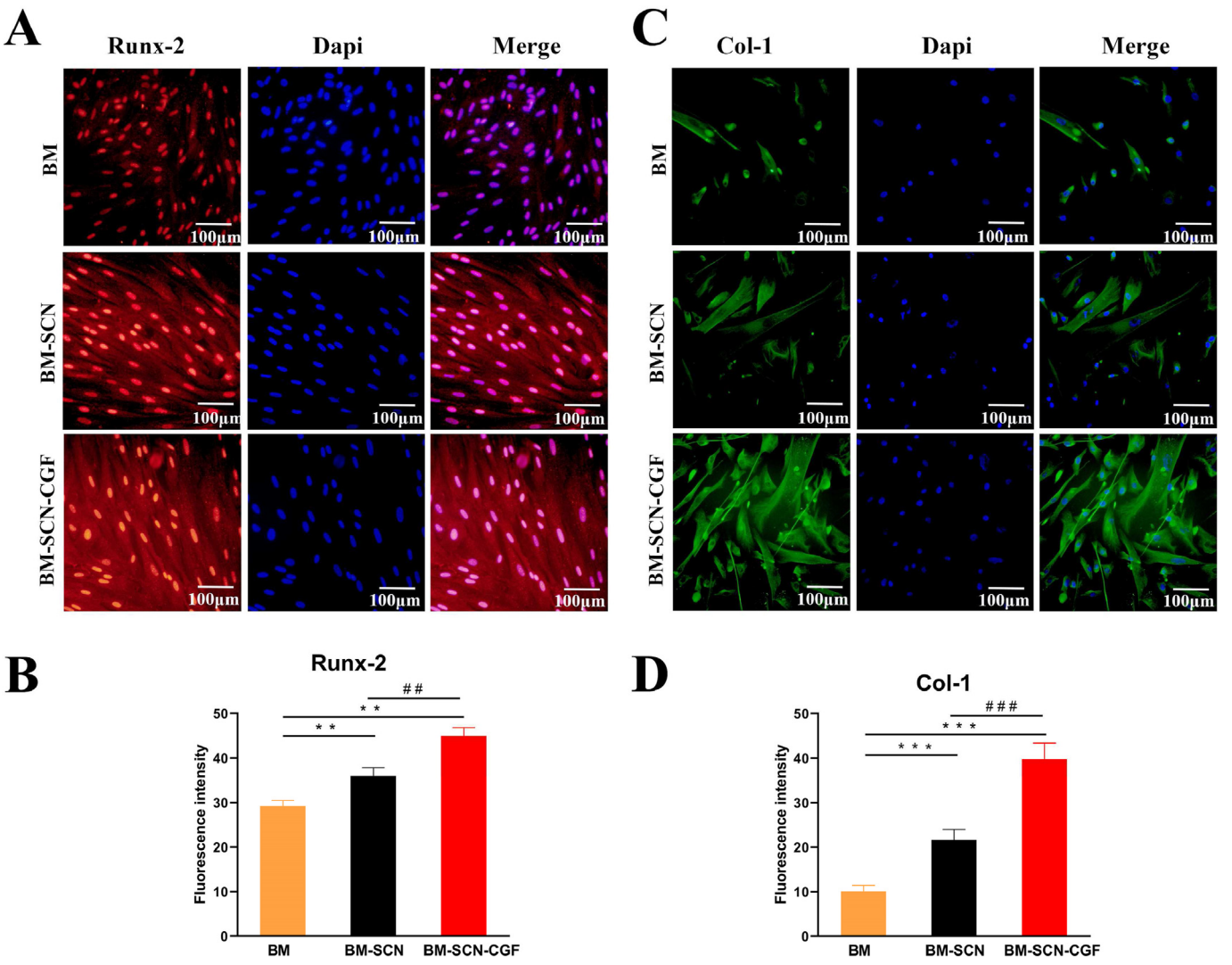

Fig. 5. The fluorescence of *Runx-2* and *Col-1* in the three groups (A) The fluorescence of *Runx-2* after 7 d of osteoinduction (B) semi-quantitative fluorescence results of expression of *Runx-2* (n = 3) (C) The fluorescence of *Col-1* after 14 d of osteoinduction (D) semi-quantitative fluorescence results of expression of *Col-1* (n = 3).**p < 0.01, ***p < 0.001 compared with the BM group, ##p < 0.01, ###p < 0.001 compared with the BM-SCN group.

addition, we used immunohistofluorescence to further verify the expression of Col-I, and the results were consistent with the immunohistochemistry results.

4. Discussion

The treatment of critical-sized bone defects remains a substantial challenge. Many studies have focused on the use of bone tissue engineering scaffolds combined with growth factors to repair critical bone defects. However, as many scaffold materials have excellent biocompatibility and most exogenous growth factors induce immune rejection to different degrees, it is difficult to translate these research results into effective clinical treatments. Recently, a model of bone biomimetic composite scaffolds synthesized from a variety of natural biomaterials combined with autologous endogenous growth factors has attracted extensive attention [26–28]. Natural organic biomaterials, such as chitosan, silk fibroin, gelatin, and collagen, have been proven to have good biocompatibility [34]. The organic–inorganic bone biomimetic scaffold constructed via combination with nHA, which is the main inorganic component of bone tissue, restores the specific structure of bone tissue to the greatest extent [7]. In addition, with the continuous improvement of extraction equipment and methods in recent years, the extraction efficiency and purity of autologous growth factors extracted from autologous blood have been greatly improved [35,36]. Due to the excellent biocompatibility of both bone biomimetic composite scaffolds and autologous endogenous growth factors, this combined model may have considerable potential for clinical translation. In our study, organic–inorganic bone biomimetic scaffolds SF/CS/nHA and autologous concentrated growth factor CGF were successfully prepared. The combination of the two promoted the proliferation and osteogenic differentiation of BMSCs in vitro and successfully repaired critical radius defects in rabbits in vivo. The combination improved the efficiency of bone regeneration.

The SF/CS/nHA scaffold was composed of CS and SF as an organic framework, and nHA was added as the main inorganic component. nHA is the most important inorganic component of bone tissue, with good osteoconductivity and mechanical strength, and a study suggested that nHA could promote the osteogenic differentiation of stem cells [37]. We prepared SF/CS/nHA scaffolds by vacuum freeze-drying combined with chemical crosslinking. The vacuum freeze-drying method maintained the stability of the scaffold structure and formed a relatively uniform internal pore size by

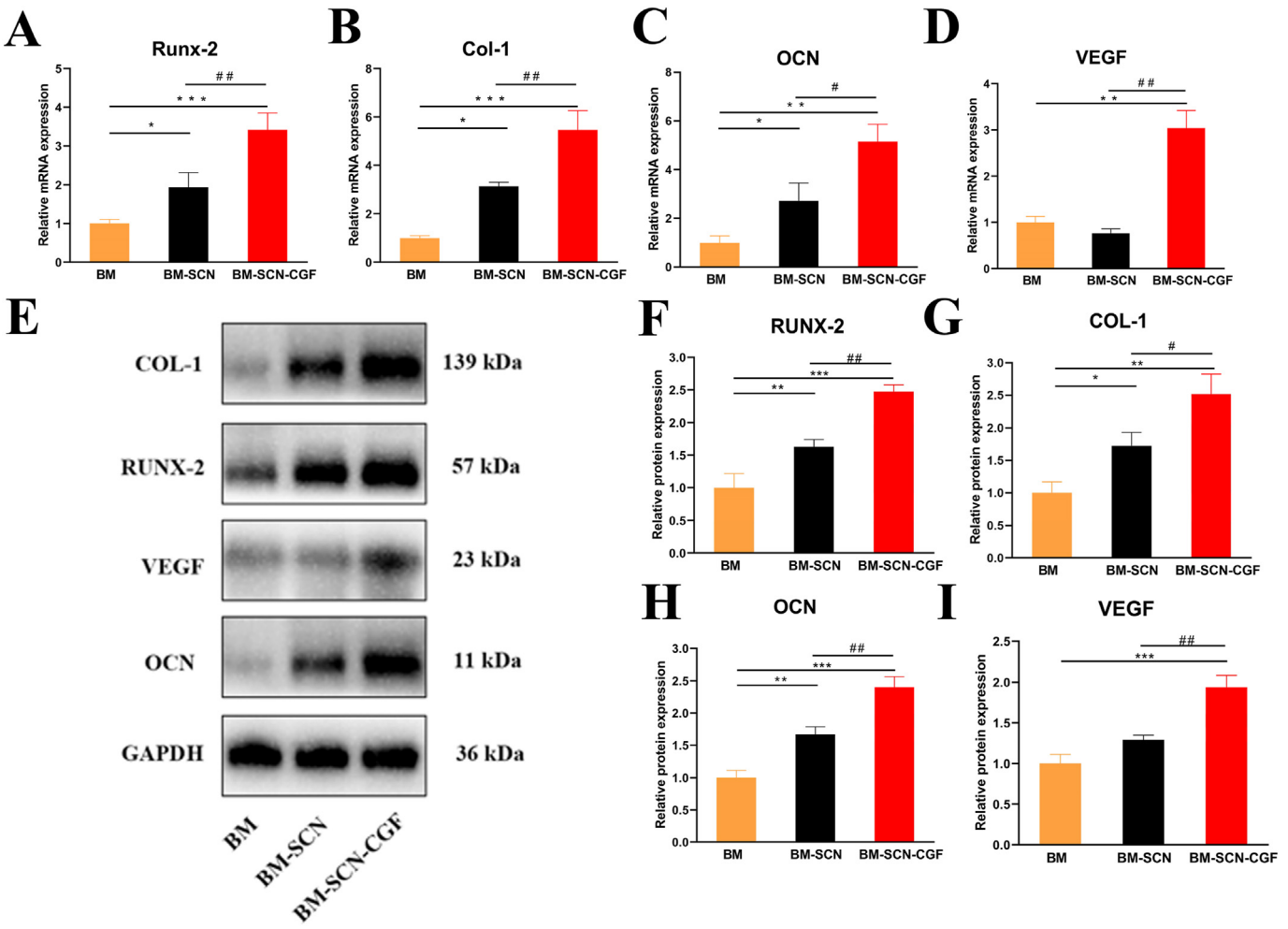

Fig. 6. Osteogenic differentiation of BMSCs at the gene and protein levels (A–D) The gene expression of *Runx-2, OCN, Col-1,* and *VEGF* after 14 d of osteoinduction (n = 3) (E) A Western blot assay was used to detect the protein expression levels of *Runx-2, OCN, Col-1,* and *VEGF* after 14 d of osteoinduction (F–I) Quantitative results of Western blot assays (n = 3). *p < 0.05, **p < 0.01, ***p < 0.001 compared with the BM group, #p < 0.05, ##p < 0.01 compared with the BM-SCN group.

alternating freezing at −80 °C and vacuum suction multiple times without adding other chemical reagents. This is considered to be an excellent method for constructing biomimetic porous scaffolds [38]. The cross-linking of CH_3OH and NaOH can convert the water-soluble α-helix structure of SF into a stable β-sheet structure. EDC and NHS are nontoxic and biocompatible cross-linking agents. They can further promote the formation of amide crosslinks between the carboxyl and amine groups in SF and CS and enable the formation of ester bonds between the activated carboxyl and hydroxyl groups; thus, the biostability of the scaffolds can be enhanced by optimizing the covalent structure of the internal molecules of the scaffolds [39,40]. nHA contains OH^-, Ca^{2+}, and P elements. Ca^{2+} can be closely combined with the carboxyl groups in CS and SF to form nanohydroxyapatite mineralized crystals, and the hydroxyl groups of nHA can form stable ester bonds with the carboxyl groups in CS and SF so that nHA is evenly distributed inside the scaffold structure. SEM electron microscopy showed that the scaffolds with three concentrations had a 3D network skeleton structure composed of SF and CS, and the particles formed by nanohydroxyapatite crystals were evenly dispersed in the 3D network skeleton structure. The pores inside the scaffold were uniform, and the porosity and pore size gradually decreased with increasing mass fraction. The compressive strength and compressive modulus increased with increasing mass fraction. After comprehensive comparison, we selected the scaffold with a mass fraction of 4% for follow-up research. The average porosity of human cancellous bone is close to 80%. Studies have shown that the porosity of bone tissue engineering scaffolds should be at least 70% to ensure the exchange of nutrients required by cells and the migration of small molecular substances [41]. The 4% SF/CS/nHA we selected had an average porosity of 83.173 ± 2.37%, which was close to the average porosity of human cancellous bone of 80%. The pore size of 100 μm–300 μm was conducive to cell adhesion and local neovascular ingrowth [42], and the average pore size of 4% SF/CS/nHA was 126.53 ± 16.11 μm, which was included in this range. The compressive strength of 4% SF/CS/nHA was 6.84 ± 0.63 MPa. There was still a difference in mechanical properties compared with normal bone tissue, but this scaffold could provide a relatively stable three-dimensional living space for cell growth, which we think is sufficient. Moreover, in practical clinical applications, in addition to filling biological scaffolds, the repair of bones requires internal fixation plates or external fixation brackets, which can ensure sufficient mechanical strength for fracture repair.

Cell adhesion, growth status, and proliferation rate are the main parameters for evaluating the biocompatibility of bionic scaffold materials. SEM showed that BMSCs grew in clusters in the SF/CS/nHA scaffold, the cell shape was an oval or a flat polygon, and the cells had protruding pseudopodia and adhered and grew well on

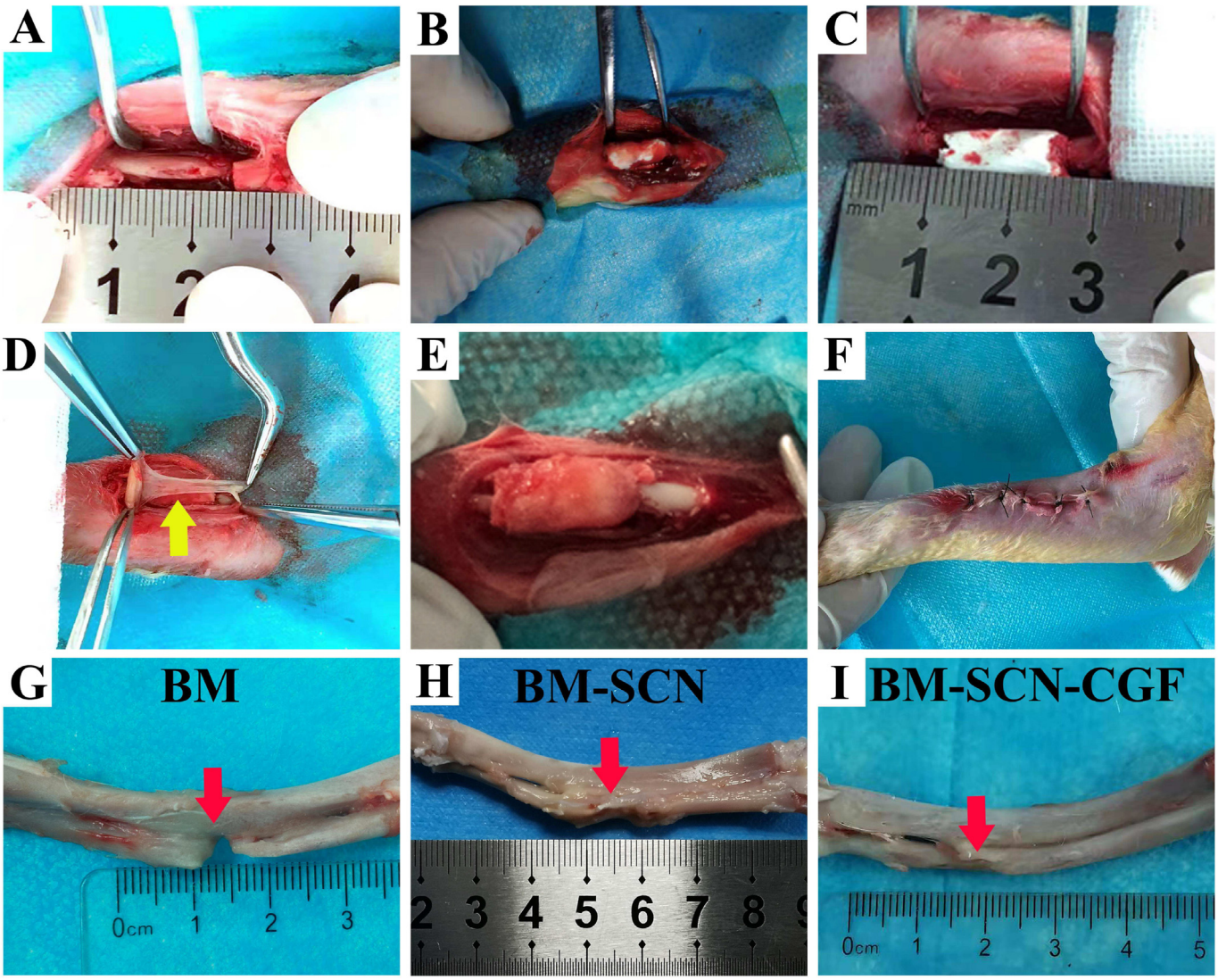

Fig. 7. Surgical procedure (A) The radial bone defect was constructed, the defects were treated with BMSCs (BM group) (B–C) The defects were treated with the scaffold-BMSC complex (BM-SCN group) (D) The defects were treated with CGF membrane combined with the scaffold-BMSC complex (BM–SCN–CGF group) (E) CGF membrane was completely coated onto the surface of the SF-CS-nHA scaffold (F) The incision was sutured (G–I) General observation of gross samples; Yellow arrow, CGF membrane; Red arrow, defects of the radius.

the scaffold. This indicated that the SF/CS/nHA scaffold had the ability to promote cell adhesion and could guide cells to grow into the scaffold to form a relatively stable scaffold cell complex. Furthermore, we also observed that some calcium salt crystals were wrapped around the cells, which was one of the hallmarks of the osteogenic differentiation of stem cells. This result suggested that SF/CS/nHA had some osteogenic induction ability. Live-dead staining showed that only a very small number of dead cells could be seen in the three groups, and a large number of BMSCs survived. This result indicated that SF/CS/nHA and CGF had no obvious cytotoxicity. Some studies have suggested that platelet-derived growth factor (PDGF) and transforming growth factor-β1 (TGF-β1) in CGF have positive effects on stem cell morphology and proliferation [43,44]. To further assess cell growth morphology, we performed phalloidin staining. Although the morphology in the BM-SCN group was worse than that in the BM group, we found that after adding 10% CGF, the morphology of BMSCs was significantly improved, and the cells were fully spread and connected into sheets. Additionally, after adding 10% CGF, the proliferation of BMSCs in the BM–SCN–CGF group was the most obvious. All these results indicated that CGF could improve cell morphology and promote cell proliferation. In addition, some studies have shown that a CGF concentration greater than 20% can inhibit the proliferation of BMSCs due to the inhibitory effect of leukocytes and inflammatory factors such as IL-6 in CGF [29,30]. Therefore, we chose a concentration of 10%.

The osteoinductive properties of scaffolds are a prerequisite for their wide application in bone repair. In the early stage of bone formation, osteoblasts secrete alkaline phosphatase (ALP) to hydrolyze phosphate esters to provide necessary phospholipids for the deposition of hydroxyapatite. ALP is one of the early indicators of osteogenic differentiation. Mature osteoblasts have significantly increased mineralization activity, and a large number of calcium nodules are deposited when they enter the stage of extracellular matrix mineralization. Calcium nodules are an important feature of late osteogenesis. ALP staining and alizarin red staining were used to evaluate early and late osteogenic effects, respectively. The ALP staining depth and the degree of cell

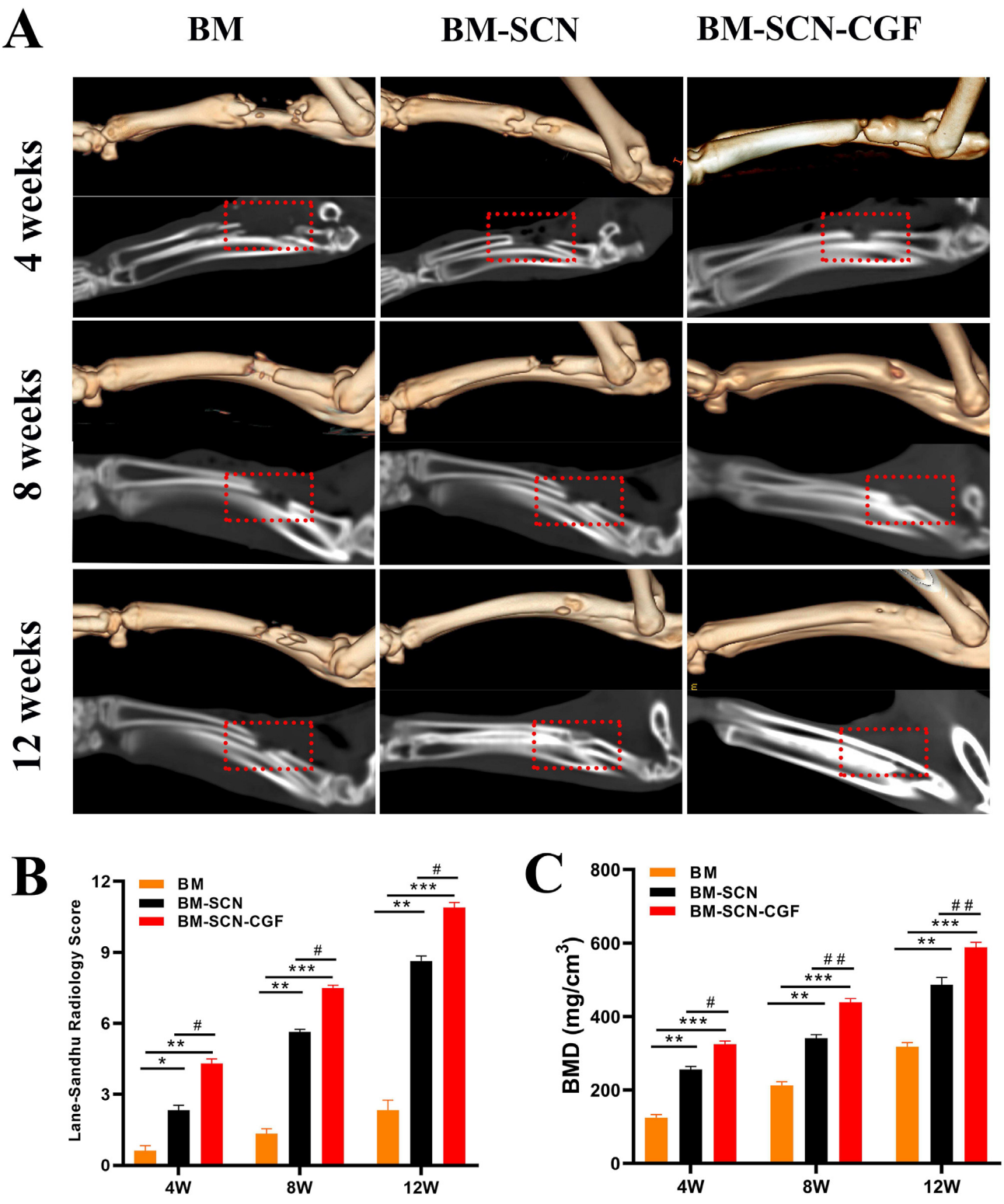

Fig. 8. The repair of bone defects was evaluated by 3D CT (A) 3D reconstruction and sagittal image at 4, 8, and 12 weeks (B) Lane-Sandhu radiology score evaluated the repair of radial bone defects among the three groups (n = 6) (C) bone mineral density of the radial bone defect area quantified by 3D-CT (n = 6); BMD, bone mineral density; *p < 0.05, **p < 0.01, ***p < 0.001 compared with BM group, #p < 0.05, ##p < 0.01 compared with the BM-SCN group.

mineralization in the BM—SCN—CGF group were significantly higher than those in the other two groups *(P < 0.05)*, while those in the BM-SCN group was significantly higher than those in the BM group *(P < 0.05)*. This may suggest that CGF could promote the osteogenic differentiation of BMSCs during the early and late stages of osteogenesis and that CGF maintained the continuity of osteogenic induction. CGF contains BMP-2, BMP-4, BMP-7, which are important growth factors for inducing osteogenic differentiation and regulating bone metabolism. A study demonstrated that the sustained and stable release of BMPs in CGF was the main

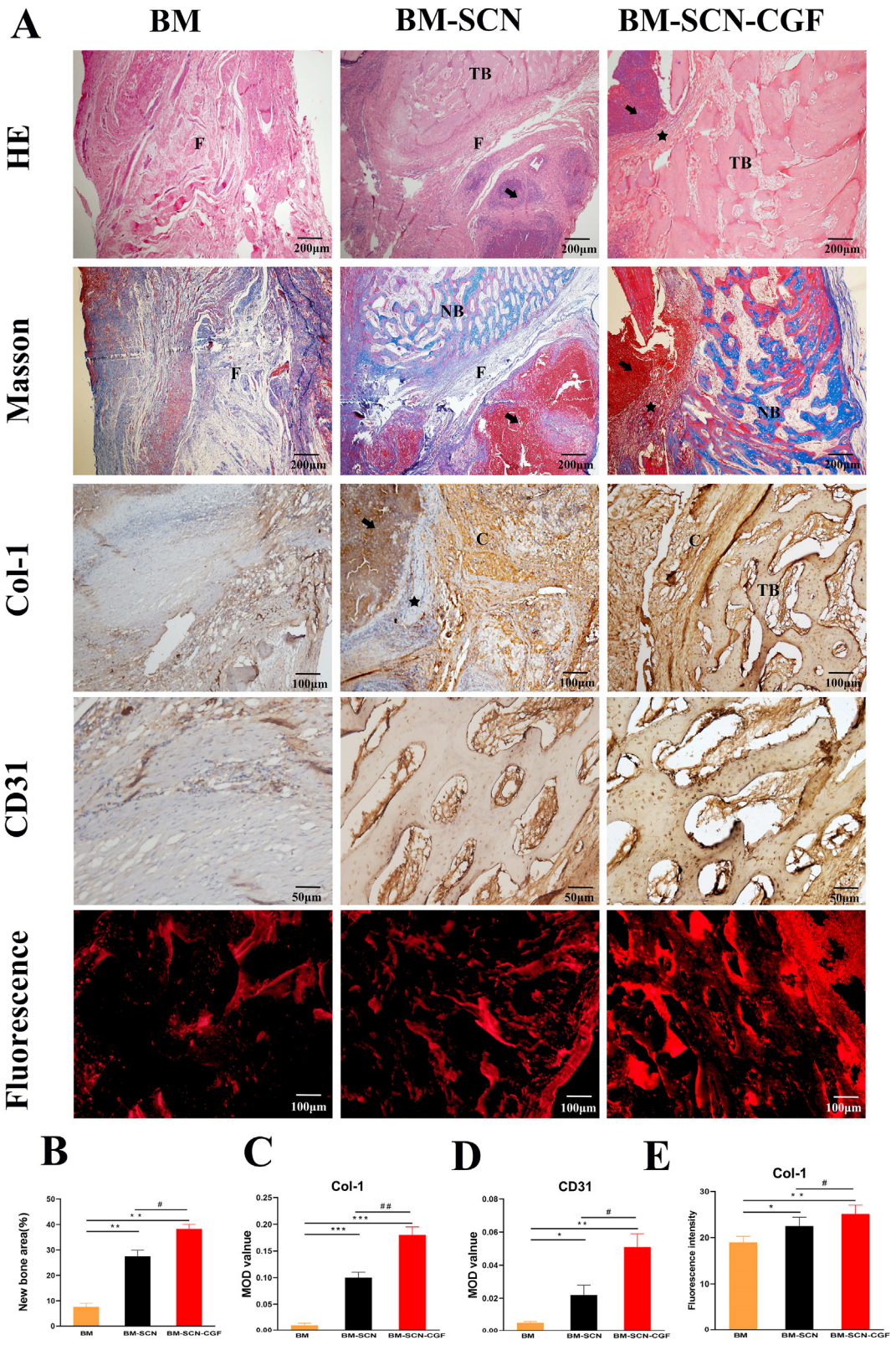

Fig. 9. Histological analysis of bone regeneration in vivo (A) Hematoxylin–eosin (HE) staining, Masson staining, immunohistochemistry of Col-1 and CD31 and immunohistofluorescence of Col-1 (B) New bone formation area quantified by Masson staining (n = 6) (C–D) Expression of COL-1 and CD31 quantified by immunohistochemistry (n = 6) (E) Expression of COL-1 quantified by immunohistofluorescence (n = 6). F, fibrous tissue; C, type I collagen; TB, trabecular bone; NB, new bone; Black arrow, remaining scaffold; Black star, transition zone between the remaining scaffold and the new bone. *p < 0.05, **p < 0.01, ***p < 0.001 compared with the BM group, #p < 0.05, ##p < 0.01 compared with the BM-SCN group.

reason for the induction of osteogenic differentiation of stem cells [45]. A recent study found that nanoparticles with nHA as the main component could induce the osteogenic differentiation of BMSCs in vitro [46]. We also found that the SF-CS-nHA scaffold itself had a certain osteogenic induction effect on BMSCs. EDS energy spectrum analysis showed that SF-CS-nHA was mainly composed of natural C and O and contained uniformly distributed Ca and P. The elements Ca and P mainly came from nHA in the scaffold. Ca and P can be directly taken in by osteoblasts to form inorganic components in the new bone matrix and participate in the formation of new bone in the implanted area. Furthermore, the hydroxyapatite mineralization crystal formed by the close combination of Ca^{2+} and the carboxyl groups in CS and SF contributed to the biomineralization of new bone tissue. These may be the reasons why SF-CS-nHA had an osteogenic induction effect.

During the process of osteogenic differentiation, cells undergo multiple differentiation steps, including the transformation phase, proliferation phase, cell aggregation and secretion phase and extracellular matrix mineralization phase. We further explored the effects of scaffold components and CGF on the osteogenic differentiation of BMSCs at different stages of osteogenesis at the gene and protein levels. Runx-2 is the initial transcription factor in the process of osteogenic differentiation. It regulates and activates the expression of a series of osteogenic genes through the TGF-β system. It is the earliest detectable and most characteristic marker protein in the process of osteogenesis [47]. Col-1 is expressed in the early and middle stages of osteogenesis and promotes phenotypic maturation of osteoblasts and initial formation of calcium nodules [48]. OCN is a polypeptide secreted by mature osteoblasts that can promote the deposition of mineralized substances in the extracellular matrix and reflect the mineralization degree of osteoblasts [49]. Cell immunofluorescence showed that Runx-2 was abundantly expressed in the cytoplasm and nucleus of BMSCs in the BM–SCN–CGF group on day 7, indicating that the osteogenic differentiation program was fully activated. COL-1 was most highly expressed in the cytoplasm of BMSCs in the BM–SCN–CGF group on day 14, indicating that CGF and scaffold components continued to induce BMSCs to enter mid-stage osteogenic differentiation. On the 14th day of osteogenic induction, we detected the expression of the three osteogenic genes Runx-2, Col-1 and OCN. The results showed that the expression levels of the three osteogenic genes in the BM–SCN–CGF group were significantly higher than those in the other two groups. This result may indicate that the osteogenic induction effects of CGF and SF-CS-nHA scaffolds were superimposed. VEGF is a characteristic marker that promotes angiogenic differentiation of stem cells. A study from Lei et al. [50] found that CGF could upregulate the expression of VEGF in stem cells through YAP pathways and promote angiogenesis in vivo. The present study found that the expression level of VEGF was only upregulated in the BM–SCN–CGF group, while the other two groups showed no VEGF upregulation. We further verified the protein expression of the above four genes by Western blotting, and the results were consistent with the PCR results. Therefore, we speculated that CGF had the dual effect of inducing osteogenesis and vascularization of stem cells at the same time, which may be difficult to achieve with other single exogenous growth factors.

Stereo-cylindrical scaffolds are a better choice than hydrogel scaffolds and thin-film fiber scaffolds for repairing long diaphyseal defects. The SF-CS-nHA scaffold is a three-dimensional columnar porous scaffold. In vivo experiments, we explored the reparative effect of SF-CS-nHA combined with CGF on critical bone defects of the rabbit radius. We chose to completely coat the SF-CS-nHA scaffold with a CGF membrane, which was inspired by the Masquelet membrane induction technique. In a study from Arıcan et al. [51], the Masquelet membrane induction technique was innovatively combined with CGF membranes, and this treatment resulted in more new bone formation than the control treatment at 12 weeks postoperatively. In our study, the nondegradable bone marrow mud in Masquelet technology was replaced with the SF-CS-nHA biomimetic biodegradable scaffold, which was implanted in the radial defect of rabbits. CGF membrane acted as an inducing membrane. CGFe was injected locally at the fracture end every week to simulate the process of physiological delivery of growth factors in vivo during bone repair. An effective concentration of CGF was maintained. We think this may be a simple system for sustained local release of growth factors. CT 3D reconstruction of the radius showed that the bone defect repair effect in the BM–SCN–CGF group was better than that in the other two groups at 4, 8, and 12 weeks after surgery. This result indicated that the SF-CS-nHA scaffold combined with CGF had a higher bone repair efficiency than other treatments in vivo. In the BM–SCN–CGF group, HE and Masson staining showed that the scaffolds were well integrated with bone tissue under the action of CGF, most of the scaffolds were effectively degraded and replaced by normal new bone tissue, and a large number of bone trabeculae were formed, accompanied by partial neovascularization. This result indicated that the SF-CS-nHA scaffold combined with CGF had excellent histocompatibility and could guide bone regeneration in vivo. Type I collagen (Col-I) is an important indicator of the development of bone mechanical strength [52]. The results of immunohistochemistry and immunofluorescence demonstrated that the expression of Col-I was the highest in the BM–SCN–CGF group. This also indicated that SF-CS-nHA scaffolds combined with CGF had a significant promoting effect on collagen formation and mineralization in the later stage of bone repair. A study found that the addition of CGF to the fracture stump resulted in a significant neovascularization effect [53]. Local angiogenesis occurs throughout the process of bone repair and reconstruction. Local vascularization can improve local blood circulation, bring nutrients to new bone tissue and cells, and accelerate bone tissue repair. CD31 is a protein that is specifically expressed during the process of angiogenesis. The expression of CD31 was highest in the BM–SCN–CGF group in vivo. We also found that the surrounding new bone tissue had more new blood vessels in the BM–SCN–CGF group. Therefore, these results suggest that CGF has the dual effect of guiding bone regeneration and promoting local vascularization, which may be its unique advantage.

5. Conclusion

A SF/CS/nHA composite biomimetic bone scaffold combined with autologous CGF promoted the proliferation and osteogenic differentiation of BMSCs in vitro and improved the repair efficiency of critical bone defects in vivo. This combination may have potential for clinical translation due to its excellent biocompatibility.

Ethical statement

The authors are accountable for all aspects of the work in ensuring that questions related to the accuracy or integrity of any part of the work are appropriately investigated and resolved. Institutional Review Board of the Third Affiliated Hospital of Zunyi Medical University has approved this study (IRB No. 2021-2-373).

Availability of data and material

The analyzed data sets generated during the present study are available from the corresponding author on reasonable request.

Funding

This work was supported by grants from the Science and Technology Fund Project of Guizhou Provincial Health Commission (No.gzwjkj2020-1-129), The United Technology Project of Zunyi City (No.HZ2022-49).

Author contributions

Yi Zhou and Bingyan Xiang conceptualized and designed the study. All authors researched, collated, and wrote this paper.

Declaration of competing interest

The authors declare no conflict of interest.

Acknowledgment

Thanks to the Science and Technology Fund Project of Guizhou Provincial Health Commission (No.gzwjkj2020-1-129) and the United Technology Project of Zunyi City (No.HZ2022-49) for the financial support of this study.

Thanks to Dr. Ling Chen for academic advice.

References

[1] Fu Z, Cui J, Zhao B, Shen SG, Lin K. An overview of polyester/hydroxyapatite composites for bone tissue repairing. J Orthop Translat 2021;28:118–30. https://doi:10.1016/j.jot.2021.02.005.

[2] Song T, Zhou J, Shi M, Xuan L, Jiang H, Lin Z, et al. Osteon-mimetic 3D nanofibrous scaffold enhances stem cell proliferation and osteogenic differentiation for bone regeneration. Biomater Sci 2022;10:1090–103. https://doi:10.1039/d1bm01489g.

[3] Wang L, Wei X, Duan C, Yang J, Xiao S, Liu H, et al. Bone marrow mesenchymal stem cell sheets with high expression of hBD3 and CTGF promote periodontal regeneration. Mater Sci Eng C Mater Biol Appl 2022:112657. https://doi:10.1016/j.msec.2022.112657.

[4] Grande F, Tucci P. Titanium dioxide nanoparticles: a risk for human Health? Mini Rev Med Chem 2016;16:762–9. https://doi:10.2174/1389557516666160321114341.

[5] Han X, Zhou X, Qiu K, Feng W, Mo H, Wang M, et al. Strontium-incorporated mineralized PLLA nanofibrous membranes for promoting bone defect repair. Colloids Surf B Biointerfaces 2019;179:363–73. https://doi:10.1016/j.colsurfb.2019.04.011.

[6] Li Y, Aparicio C. Discerning the subfibrillar structure of mineralized collagen fibrils: a model for the ultrastructure of bone. PLoS One 2013;8:e76782. https://doi: 10.1371/journal.pone.0076782.

[7] Song T, Zhao F, Wang Y, Li D, Lei N, Li X, et al. Constructing a biomimetic nanocomposite with the in situ deposition of spherical hydroxyapatite nanoparticles to induce bone regeneration. J Mater Chem B 2021;9:2469–82. https://doi: 10.1039/d0tb02648d.

[8] Zhao H, Zhang Y, Liu Y, Zheng P, Gao T, Cao Y, et al. In situ forming cellulose nanofibril-reinforced hyaluronic acid hydrogel for cartilage regeneration. Biomacromolecules 2021;22:5097–107. https://doi: 10.1021/acs.biomac.1c01063.

[9] Zhan Y, Deng B, Wu H, Xu C, Wang R, Li W, et al. Biomineralized composite liquid crystal fiber scaffold promotes bone regeneration by enhancement of osteogenesis and angiogenesis. Front Pharmacol 2021;12:736301. https://doi:10.3389/fphar.2021.736301.

[10] Hassanzadeh A, Ashrafihelan J, Salehi R, Rahbarghazi R, Firouzamandi M, Ahmadi M, et al. Development and biocompatibility of the injectable collagen/nano-hydroxyapatite scaffolds as in situ forming hydrogel for the hard tissue engineering application. Artif Cell Nanomed Biotechnol 2021;49:136–46. https://doi: 10.1080/21691401.2021.1877153.

[11] Madhavasarma P, Veeraragavan P, Kumaravel S, Sridevi M. Studies on physiochemical modifications on biologically important hydroxyapatite materials and their characterization for medical applications. Biophys Chem 2020;267:106474. https://doi: 10.1016/j.bpc.2020.106474.

[12] Guo J, Yang B, Ma Q, Fometu SS, Wu G. Photothermal regenerated fibers with enhanced toughness: silk fibroin/MoS2 nanoparticles. Polymers 2021;13:3937–43. https://doi: 10.3390/polym13223937.

[13] Khosropanah MH, Vaghasloo MA, Shakibaei M, Mueller AL, Kajbafzadeh AM, Amani L, et al. Biomedical applications of silkworm (Bombyx Mori) proteins in regenerative medicine (a narrative review). J Tissue Eng Regen Med 2022;16:91–109. https://doi: 10.1002/term.3267.

[14] Ambaye TG, Vaccari M, Prasad S, van Hullebusch ED, Rtimi S. Preparation and applications of chitosan and cellulose composite materials. J Environ Manage 2022;301:113850. https://doi: 10.1016/j.jenvman.2021.113850.

[15] Guo J, Chen C, Chen W, Jiang J, Chen B, Zheng F. Effective immobilization of Bacillus subtilis in chitosan-sodium alginate composite carrier for ammonia removal from anaerobically digested swine wastewater. Chemosphere 2021;284:131266. https://doi: 10.1016/j.chemosphere.2021.131266.

[16] Xiao H, Huang W, Xiong K, Ruan S, Yuan C, Mo G, et al. Osteochondral repair using scaffolds with gradient pore sizes constructed with silk fibroin, chitosan, and nano-hydroxyapatite. Int J Nanomedicine 2019;14:2011–27. https://doi:10.2147/IJN.S191627.

[17] Shah NJ, Hyder MN, Quadir MA, Dorval Courchesne NM, Seeherman HJ, Nevins M, et al. Adaptive growth factor delivery from a polyelectrolyte coating promotes synergistic bone tissue repair and reconstruction. Proc Natl Acad Sci U S A 2014;111:12847–52. https://doi: 10.1073/pnas.1408035111. Epub 2014 Aug 18.

[18] Borsani E, Buffoli B, Bonazza V, Brunelli G, Monini L, Inchingolo F, et al. In vitro effects of concentrated growth factors (CGF) on human SH-SY5Y neuronal cells. Eur Rev Med Pharmacol Sci 2020;24:304–14. https://doi: 10.26355/eurrev_202001_19927.

[19] Tabatabaei F, Aghamohammadi Z, Tayebi L. In vitro and in vivo effects of concentrated growth factor on cells and tissues. J Biomed Mater Res 2020;108:1338–50. https://doi.org/10.1002/jbm.a.36906.

[20] Rodella LF, Favero G, Boninsegna R, Buffoli B, Labanca M, Scarì G, et al. Growth factors, CD34 positive cells, and fibrin network analysis in concentrated growth factors fraction. Microsc Res Tech 2011;74:772–7. https://doi: 10.1002/jemt.20968.

[21] Rochira A, Siculella L, Damiano F, Palermo A, Ferrante F, Carluccio MA, et al. Concentrated growth factors (CGF) induce osteogenic differentiation in human bone marrow stem cells. Biology 2020;9:370. https://doi: 10.3390/biology9110370.

[22] Yamaguchi S, Aizawa H, Sato A, Tsujino T, Isobe K, Kitamura Y, et al. Concentrated growth factor matrices prepared using Silica-coated plastic tubes are distinguishable from those prepared using Glass tubes in platelet distribution: application of a novel near-infrared imaging-based, quantitative technique. Front Bioeng Biotechnol 2020;8:600–8. https://doi: 10.3389/fbioe.2020.00600.

[23] Masuki H, Okudera T, Watanebe T, Suzuki M, Nishiyama K, Okudera H, et al. Growth factor and pro-inflammatory cytokine contents in platelet-rich plasma (PRP), plasma rich in growth factors (PRGF), advanced platelet-rich fibrin (A-PRF), and concentrated growth factors (CGF). Int J Implant Dent 2016;2:19–27. https://doi: 10.1186/s40729-016-0052-4.

[24] Aizawa H, Tsujino T, Watanabe T, Isobe K, Kitamura Y, Sato A, et al. Quantitative near-infrared imaging of platelets in platelet-rich fibrin (PRF) matrices: comparative analysis of bio-PRF, leukocyte-rich PRF, advanced-PRF and concentrated growth factors. Int J Mol Sci 2020;21:4426–35. https://doi: 10.3390/ijms21124426.

[25] Kang YH, Jeon SH, Park JY, Chung JH, Choung YH, Choung HW, et al. Platelet-rich fibrin is a Bioscaffold and reservoir of growth factors for tissue regeneration. Tissue Eng Part A 2011;17:349–59. https://doi: 10.1089/ten.TEA.2010.0327.

[26] Wang X, Tong S, Huang S, Ma L, Liu Z, Zhang D. Application of a new type of natural calcined bone repair material combined with concentrated growth factors in bone regeneration in rabbit critical-sized calvarial defect. BioMed Res Int 2020;2020:8810747. https://doi: 10.1155/2020/8810747.

[27] Fang D, Long Z, Hou J. Clinical application of concentrated growth factor fibrin combined with bone repair materials in jaw defects. J Oral Maxillofac Surg 2020;78:882–92. https://doi: 10.1016/j.joms.2020.01.037.

[28] Dai Y, Han XH, Hu LH, Wu HW, Huang SY, Lü YP. Efficacy of concentrated growth factors combined with mineralized collagen on quality of life and bone reconstruction of guided bone regeneration. Regen Biomater 2020;7:313–20. https://doi: 10.1093/rb/rbaa007.

[29] Chen X, Chen Y, Hou Y, Song P, Zhou M, Nie M, et al. Modulation of proliferation and differentiation of gingiva-derived mesenchymal stem cells by concentrated growth factors: potential implications in tissue engineering for dental regeneration and repair. Int J Mol Med 2019;44:37–46. https://doi: 10.3892/ijmm.2019.4172.

[30] Honda H, Tamai N, Naka N, Yoshikawa H, Myoui A. Bone tissue engineering with bone marrow-derived stromal cells integrated with concentrated growth factor in Rattus norvegicus calvaria defect model. J Artif Organs 2013;16:305–15. https://doi: 10.1007/s10047-013-0711-7.

[31] Leng Y, Ren G, Cui Y, Peng C, Wang J, Wu D, et al. Platelet-rich plasma-enhanced osseointegration of decellularized bone matrix in critical-size radial defects in rabbits. Ann Transl Med 2020;8:198–204. https://doi.org/10.21037/atm.2020.01.53.

[32] Liu Z, Chu W, Zhang L, Wang Y, Zhai Z, Liu F. The effect of enhanced bone marrow in conjunction with 3D-printed PLA-HA in the repair of critical-sized bone defects in a rabbit model. Ann Transl Med 2021;9:1134–41. https://doi.org/10.21037/atm-20-8198.

[33] Sun H, Godbout C, Ryan G, Hoit G, Higgins J, Schemitsch EH. The induced membrane technique: optimization of bone grafting in a rat model of segmental bone defect. Injury 2022;53:1848–53. https://doi.org/10.1016/j.injury.2022.03.023.

[34] Kim JW, Han YS, Lee HM, Kim JK, Kim YJ. Effect of morphological characteristics and biomineralization of 3D-printed gelatin/hyaluronic acid/hydroxyapatite composite scaffolds on bone tissue regeneration. Int J Mol Sci 2021;22:6792–9. https://doi: 10.3390/ijms22136794.

[35] Li W, Wang F, Dong F, Zhang Z, Song P, Chen H, et al. CGF membrane promotes periodontal tissue regeneration mediated by hUCMSCs through upregulating

TAZ and osteogenic differentiation genes. Stem Cells Int 2021;2021:6644366. https://doi: 10.1155/2021/6644366.
[36] Bonazza V, Borsani E, Buffoli B, Castrezzati S, Rezzani R, Rodella LF. How the different material and shape of the blood collection tube influences the Concentrated Growth Factors production. Microsc Res Tech 2016;79:1173–8. https://doi: 10.1002/jemt.22772.
[37] Fang CH, Sun CK, Lin YW, Hung MC, Lin HY, Li CH, et al. Metformin-Incorporated gelatin/nano-hydroxyapatite scaffolds promotes bone regeneration in critical size rat alveolar bone defect model. Int J Mol Sci 2022;23:558–64. https://doi: 10.3390/ijms23010558.
[38] Sun K, Li R, Jiang W, Sun Y, Li H. Comparison of three-dimensional printing and vacuum freeze-dried techniques for fabricating composite scaffolds. Biochem Biophys Res Commun 2016;477:1085–91. https://doi: 10.1016/j.bbrc.2016.07.050.
[39] Li DW, He J, He FL, Liu YL, Liu YY, Ye YJ, et al. Silk fibroin/chitosan thin film promotes osteogenic and adipogenic differentiation of rat bone marrow-derived mesenchymal stem cells. J Biomater Appl 2018;32:1164–73. https://doi: 10.1177/0885328218757767.
[40] Singh BN, Pramanik K. Fabrication and evaluation of non-mulberry silk fibroin fiber reinforced chitosan based porous composite scaffold for cartilage tissue engineering. Tissue Cell 2018;55:83–90. https://doi: 10.1016/j.tice.2018.10.003.
[41] David N, Nallaiyan R. Biologically anchored chitosan/gelatin-SrHAP scaffold fabricated on Titanium against chronic osteomyelitis infection. Int J Biol Macromol 2018;110:206–14. https://doi: 10.1016/j.ijbiomac.2017.11.174.
[42] Brennan CM, Eichholz KF, Hoey DA. The effect of pore size within fibrous scaffolds fabricated using melt electrowriting on human bone marrow stem cell osteogenesis. Biomed Mater 2019;14:065016. https://doi: 10.1088/1748-605X/ab49f2.
[43] Wang J, You J, Gong D, Xu Y, Yang B, Jiang C. PDGF-BB induces conversion, proliferation, migration, and collagen synthesis of oral mucosal fibroblasts through PDGFR-β/PI3K/AKT signaling pathway. Cancer Biomark 2021;30:407–15. https://doi: 10.3233/CBM-201681.
[44] Mishima Y, Oka A, Ishihara S. Detection and quantification of transforming growth factor-β1 produced by murine B cells: pros and cons of different techniques. Methods Mol Biol 2021;2270:113–24. https://doi: 10.1007/978-1-0716-1237-8_7.
[45] Tian S, Wang J, Dong F, Du N, Li W, Song P, et al. Concentrated growth factor promotes dental pulp cells proliferation and mineralization and facilitates recovery of dental pulp tissue. Med Sci Monit 2019;25:10016–28. https://doi.org/10.12659/MSM.919316.
[46] Song T, Zhao F, Wang Y, Li D, Lei N, Li X, et al. Constructing a biomimetic nanocomposite with the in situ deposition of spherical hydroxyapatite nanoparticles to induce bone regeneration. J Mater Chem B 2021;9:2469–82. https://doi: 10.1039/d0tb02648d.
[47] Chen S, Liang H, Ji Y, Kou H, Zhang C, Shang G, et al. Curcumin modulates the crosstalk between macrophages and bone mesenchymal stem cells to ameliorate osteogenesis. Front Cell Dev Biol 2021;9:634650. https://doi: 10.3389/fcell.2021.634650.
[48] Li L, Yu M, Li Y, Li Q, Yang H, Zheng M, et al. Synergistic anti-inflammatory and osteogenic n-HA/resveratrol/chitosan composite microspheres for osteoporotic bone regeneration. Bioact Mater 2020;6:1255–66. https://doi: 10.1016/j.bioactmat.2020.10.018.
[49] Mizokami A, Kawakubo-Yasukochi T, Hirata M. Osteocalcin and its endocrine functions. Biochem Pharmacol 2017;132:1–8. https://doi: 10.1016/j.bcp.2017.02.001.
[50] Qi L, Liu L, Hu Y, Li J, Li J, Cao N, et al. Concentrated growth factor promotes gingival regeneration through the AKT/Wnt/β-catenin and YAP signaling pathways. Artif Cell Nanomed Biotechnol 2020;48:920–32. https://doi: 10.1080/21691401.2020.1773482.
[51] Arıcan G, Özmeriç A, Fırat A, Kaymaz F, Ocak M, Çelik HH, et al. Micro-ct findings of concentrated growth factors (cgf) on bone healing in masquelet's technique-an experimental study in rabbits. Arch Orthop Trauma Surg 2022;142:83–90. https://doi: 10.1007/s00402-020-03596-z.
[52] Sadeghzadeh H, Mehdipour A, Dianat-Moghadam H, Salehi R, Khoshfetrat AB, Hassani A, et al. PCL/Col I-based magnetic nanocomposite scaffold provides an osteoinductive environment for ADSCs in osteogenic cues-free media conditions. Stem Cell Res Ther 2022;13:143–51. https://doi.org/10.1186/s13287-022-02816-0.
[53] Yılmaz O, Özmeriç A, Alemdaroğlu KB, Celepli P, Hücümenoğlu S, Şahin Ö. Effects of concentrated growth factors (CGF) on the quality of the induced membrane in Masquelet's technique - an experimental study in rabbits. Injury 2018;49:1497–503. https://doi: 10.1016/j.injury.2018.06.011.